

# Nonlinear Double-Capacitor Model for Rechargeable Batteries: Modeling, Identification and Validation

Ning Tian, *Student Member, IEEE*, Huazhen Fang, *Member, IEEE*, Jian Chen, *Senior Member, IEEE*, and Yebin Wang, *Member, IEEE*

**Abstract**—This paper proposes a new equivalent circuit model for rechargeable batteries by modifying a double-capacitor model proposed in [1]. It is known that the original model can address the rate capacity effect and energy recovery effect inherent to batteries better than other models. However, it is a purely linear model and includes no representation of a battery’s nonlinear phenomena. Hence, this work transforms the original model by introducing a nonlinear-mapping-based voltage source and a serial RC circuit. The modification is justified by an analogy with the single-particle model. Two parameter estimation approaches, termed 1.0 and 2.0, are designed for the new model to deal with the scenarios of constant-current and variable-current charging/discharging, respectively. In particular, the 2.0 approach proposes the notion of Wiener system identification based on maximum *a posteriori* estimation, which allows all the parameters to be estimated in one shot while overcoming the nonconvexity or local minima issue to obtain physically reasonable estimates. An extensive experimental evaluation shows that the proposed model offers excellent accuracy and predictive capability. A comparison against the Rint and Thevenin models further points to its superiority. With high fidelity and low mathematical complexity, this model is beneficial for various real-time battery management applications.

**Index Terms**—Batteries, equivalent circuit model, nonlinear double-capacitor model, parameter identification, experimental validation.

## I. INTRODUCTION

**R**ECHARGEABLE batteries have seen an ever-increasing use in today’s industry and society as power sources for systems of different scales, ranging from consumer electronics to electric vehicles and grid-scale energy storage. This trend has motivated a growing body of research on advanced battery management algorithms, which are aimed to ensure the performance, safety and life of battery systems. Such algorithms generally require mathematical models that can well characterize a battery’s dynamics. Battery modeling thus has attracted significant attention during the past years, with the current literature offering a plethora of results.

Ning Tian and Huazhen Fang are with the Department of Mechanical Engineering, University of Kansas, Lawrence, KS 66045, USA (e-mail: ning.tian@ku.edu, fang@ku.edu).

Jian Chen is with the State Key Laboratory of Industrial Control Technology, College of Control Science and Engineering, Zhejiang University, Hangzhou, 310027, China (e-mail: jchen@zju.edu.cn).

Yebin Wang is with the Mitsubishi Electric Research Laboratories, Cambridge, MA 02139, USA (e-mail: yebinwang@merl.com).

There are two main types of battery models: 1) electrochemical models that build on electrochemical principles to characterize the electrochemical reactions and physical phenomena inside a battery during charging/discharging, and 2) equivalent circuit models (ECMs) that replicate a battery’s current-voltage characteristics using electrical circuits made of resistors, capacitors and voltage sources. With structural simplicity, the latter provides great computational efficiency, thus suitable for real-time battery management. However, as the other side of the coin, the simple circuit-based structures also imply a difficulty to capture a battery’s dynamic behavior at a high accuracy. Therefore, this work aims to develop a new ECM based on the one in [1] so that it can offer high fidelity at low mathematical complexity, through systematically investigating the model construction, parameter identification, and experimental validation.

## A. Literature Review

1) *Review of Battery Modeling*: As mentioned above, the electrochemical models and ECMs constitute the majority of the battery models available today. The electrochemical modeling approach seeks to characterize the physical and chemical mechanisms underlying the charging/discharging processes. One of the best-known electrochemical models is the Doyle-Fuller-Newman model, which describes the concentrations and transport of lithium-ions together with the distribution of separate potential in porous electrodes and electrolyte [2]–[4]. While delineating and reproducing a battery’s behavior accurately, this model, like many others of similar kind, involves a great many of partial differential equations and causes high computational costs. Even though simplified versions, e.g., the single-particle model (SPM), or some model reduction methods have been developed [4]–[6], it may still not be enough to ensure real-time monitoring and control of battery operation.

By contrast, the ECMs can be executed well in real time and have found their way into various battery management systems. The first ECM to our knowledge is the Randles model proposed in the 1940s [7]. It reveals a lead-acid battery’s ohmic and reactive (capacitive and inductive) resistance, demonstrated in the electrochemical reactions and contributing to various phenomena of voltage dynamics, e.g., voltage drop, recovery and associated transients. This model

has become a de facto standard for interpreting battery data obtained from electrochemical impedance spectroscopy [8]. It also provides a basis for building diverse ECMs to grasp a battery's voltage dynamics during charging/discharging. Adding a voltage source representing the open-circuit voltage (OCV) to the Randles model, one can obtain the popular Thevenin model [9]–[11]. Removing its resistance-capacitance (RC) circuit, the Thevenin model reduces to the simple so-called Rint model that includes an ideal voltage source with a series resistor [10]. Adding one or more RC circuits to the series, it becomes the dual polarization (DP) model that is capable of capturing multi-time-scale voltage transients during charging/discharging [10].

The literature has also reported a few modifications of the Thevenin model to better characterize a battery's dynamics. Generally, they are based on two approaches. The first one aims to describe a battery's voltage more accurately by incorporating certain phenomena, e.g., hysteresis, into the voltage dynamics, or through different parameterizations of the OCV with respect to the state-of-charge (SoC) [12]–[18]. Some literature also models the resistors and capacitors as dependent on the SoC, as well as some other factors like the temperature or rate and direction of the current loads in order to improve the accuracy of battery voltage prediction [19], [20]. The second approach sets the focus on improving the runtime prediction for batteries. In [21], a battery's capacity change due to cycle and temperature is considered and parameterized, and the dependence of resistors and capacitors on SoC also characterized. A similar investigation is made in [22] to improve the Thevenin model, which proposes to capture the nonlinear change of a battery's capacity with respect to the current load.

An ECM that shows emerging importance is a double-capacitor model [1], [23]. It consists of two capacitors configured in parallel, which correspond to an electrode's bulk inner part and surface region, respectively, and can describe the process of charge diffusion and storage in a battery's electrode. Compared to the Thevenin model, this unique circuit structure allows the rate capacity effect and charge recovery effect to be captured, making this model an attractive choice for charging control [24], [25]. However, based on a purely linear circuit, this model lacks the capability of delineating nonlinear phenomena that a battery innately demonstrates. The presented work is thus motivated to remove this limitation by revamping the model's structure.

2) *Review of Battery Model Identification*: A key problem associated with battery modeling is parameter identification, which pertains to extracting the unknown model parameters from the measurement data. Due to its importance, recent years have seen a growth of research. The existing methods can be divided into two main categories, experiment-based and data-based. The first category conducts experiments of charging, discharging or electrochemical impedance spectroscopy (EIS) and utilizes the experimental data to read a model's parameters. It is pointed out in [26]–[28] that the transient voltage responses under constant- or pulse-current charging/discharging can be leveraged to estimate the resistance, capacitance and time constant parameters of the Thevenin

model. In addition, the relation between the SoC and OCV is a defining characteristic of a battery's dynamics. It can be experimentally identified by charging or discharging a battery using a very small current [29], or alternatively, using a current of normal magnitude but intermittently (with a sufficiently long rest period applied between two discharging operations) [30], [31]. The EIS experiments have also been widely used to identify a battery's impedance properties [32]–[34]. While involving basic data analysis, the methods of this category generally put emphasis on the design of experiments. In a departure, the second category goes deeper into understanding the model-data relationship and pursues data-driven parameter estimation. It can enable provably correct identification even for complex models, thus often acknowledged as better at extracting the potential of data. It is proposed in [35] to identify the Thevenin model by solving a set of linear and polynomial equations. Another popular means is to formulate model-data fitting problems and solve them using least squares or other optimization methods to estimate the parameters [36]–[41]. When considering more complicated electrochemical models, the identification usually involves large-size nonlinear nonconvex optimization problems. In this case, particle swarm optimization and genetic algorithms are often exploited to search for the best parameter estimates [3], [42]–[44]. A recent study presents an adaptive-observer-based parameter estimation scheme for an electrochemical model [45]. While the above works focus on identification of physics-based models, data-driven black-box identification is also examined in [46]–[48], which construct linear state-space models *via* subspace identification or nonparametric frequency domain analysis. A topic related with identification is experiment design, which is to find out the best input sequences to excite a battery to maximize the parameter identifiability. In [49], [50], optimal input design is performed by maximizing the Fisher information matrices—an identifiability metric—involved in the identification of the Thevenin model and the SPM, respectively.

The presented work is also related with the literature on Wiener system identification, because the model to be developed has a Wiener-type structure featuring a linear dynamic subsystem in cascade with a static nonlinear subsystem. Wiener systems are an important subject in the field of parameter identification, and a reader is referred to [51] for a collection of recent studies. Wiener system identification based on maximum likelihood (ML) estimation is investigated in [52], [53], which shows significant promises. However, the optimization procedure resulting from the ML formulation can easily converge to local minima due to the presence of the nonlinear subsystem. This hence yields a motivation to enhance the notion of ML-based identification in this work to achieve more effective battery parameter estimation.

## B. Statement of Contributions

This work presents the following contributions.

- A new ECM, named *nonlinear double-capacitor (NDC) model*, is developed. Transforming the linear double-capacitor model in [1], the NDC model introduces a nonlinear voltage source, which is expressed as a nonlinear

mapping of the voltage across the capacitor corresponding to the surface region of a battery's electrode. This pivotal change makes it able to capture the nonlinear voltage dynamics, thus addressing a critical deficiency of the original model. It is interestingly found that, with this change, the NDC model can be interpreted as a circuit-based approximate simplification of the SPM, which provides a justification of its soundness. In addition, an RC circuit is added to describe the voltage transients associated with charge transfer inside and on the surface of an electrode.

- Parameter identification is investigated for the proposed model. This begins with a study of the constant-current charging/discharging scenario, with an identification approach, termed 1.0, developed by fitting parameters with the measurement data. Then, shifting the focus to the scenario of variable-current charging/discharging, the study introduces a Wiener perspective into the identification of the NDC model due to its Wiener-type structure. A Wiener identification approach is proposed for the NDC model based on maximum *a posteriori* (MAP) estimation, which is termed 2.0. Compared to the ML-based counterparts in the literature, this new approach incorporates into the estimation a prior distribution of the unknown parameters, which represents additional information or prior knowledge and can help drive the parameter search toward physically reasonable values.
- Experimental validation is performed to assess the proposed results. This involves multiple experiments about battery discharging under different kinds of current profiles and a comparison of the NDC model with the Rint and Thevenin models. The validation shows the considerable accuracy and predictive capability of the NDC model, as well as the effectiveness of the 1.0 and 2.0 identification approaches.

### C. Organization

The remainder of the paper is organized as follows. Section II presents the construction of the NDC model. Section III studies parameter identification for the NDC model in the constant-current charging scenario. Inspired by Wiener system identification, Section IV proceeds to develop an MAP-based parameter estimation approach to identify the NDC model. Section V offers the experimental validation. Finally, Section VI gathers concluding remarks and suggestions for future research.

## II. NDC MODEL DEVELOPMENT

This section develops the NDC model and presents the mathematical equations governing its dynamic behavior.

To begin with, let us review the original linear double-capacitor model proposed in [1]. As shown in Figure 1(a), this model includes two capacitors in parallel,  $C_b$  and  $C_s$ , each connected with a serial resistor,  $R_b$  and  $R_s$ , respectively. The double-capacitors simulate a battery's electrode, providing storage for electric charge, and the parallel connection between them allows the migration of charge within the electrode to

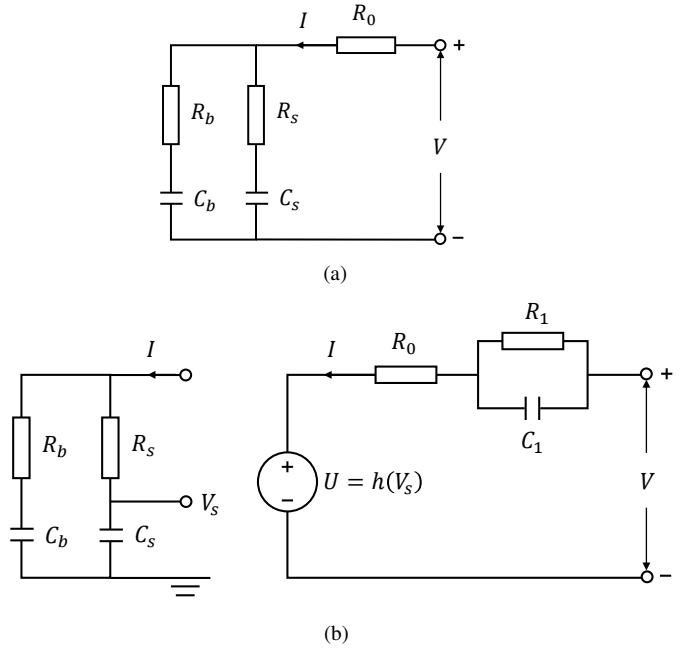


Figure 1: (a) The original double-capacitor model; (b) the proposed nonlinear double-capacitor (NDC) model.

be described. Specifically, one can consider the  $R_s$ - $C_s$  circuit as corresponding to the electrode surface region exposed to the electrolyte; the  $R_b$ - $C_b$  circuit represents an analogy of the bulk inner part of the electrode. As such, this model has the following features:

- $C_b \gg C_s$  and  $R_b \gg R_s$ ;
- $C_b$  is where the majority of the charge is stored, and  $R_b$ - $C_b$  accounts for low-frequency responses during charging/discharging;
- $C_s$  is much smaller, and its voltage changes at much faster rates than that of  $C_b$  during charging/discharging, making  $R_s$ - $C_s$  responsible for high-frequency responses.

In addition,  $R_0$  is included to embody the electrolyte resistance.

*Remark 1:* While this model was designed in [1] for high-power lithium-ion batteries, its application can naturally extend to double-layer capacitors widely used in hybrid energy storage systems, e.g., [54].

As pointed out in [24], the linear double-capacitor model can grasp the rate capacity effect, i.e., the total charge absorbed (or released) by a battery goes down with the increase in charging (or discharging) current. To see this, just notice that the terminal voltage  $V$  mainly depends on  $V_s$  (the voltage across  $C_s$ ), which changes faster than  $V_b$  (the voltage across  $C_b$ ). Thus, when the current  $I$  is large, the fast rise (or decline) of  $V_s$  will make  $V$  hit the cut-off threshold earlier than when  $C_b$  has yet to be fully charged (or discharged). Another phenomenon that can be seized is the capacity and voltage recovery effect. That is, the usable capacity and terminal voltage would increase upon the termination of discharging due to the migration of charge from  $C_b$  to  $C_s$ . However, this model by nature is a linear system, unable to describe a defining characteristic of batteries—the nonlinear dependence of the OCV on the SoC. It hence is effective only when

a battery is restricted to operate conservatively within some truncated SoC range that permits a linear approximation of the SoC-OCV curve.

To overcome the above issue, the NDC model is proposed, which is shown in Figure 1(b). It includes two changes. The primary one is to introduce a voltage source  $U$ , which is a nonlinear mapping of  $V_s$ , i.e.,  $U = h(V_s)$ . Second, an RC circuit,  $R_1-C_1$ , is added in series to  $U$ . Next, let us justify the above modifications from a perspective of the SPM, a simplified electrochemical model that has recently attracted wide interest.

Figure 2 gives a schematic diagram of the SPM. The SPM represents an electrode as a single spherical particle. It describes the mass balance and migration of lithium-ions in a particle during charging/discharging by Fick's second law of diffusion in a spherical coordinate system [5]. If subdividing a spherical particle into two finite volumes, the bulk inner domain (core) and the near-surface domain (shell), one can simplify the diffusion of lithium-ions between them as the charge transport between the capacitors of the double-capacitor model, as proven in [24]. For SPM, the terminal voltage consists of three elements: the difference in the open-circuit potential of the positive and negative electrodes, the difference in the reaction overpotential, and the voltage across the film resistance [4]. The reaction overpotential difference is almost negligible when the input current is not large. In addition, the open-circuit potential depends on the lithium-ion concentration in the surface region of the sphere, which is akin to the role  $V_s$  here. Therefore, it is appropriate as well as necessary to introduce a nonlinear function of  $V_s$  as an analogy to the open-circuit potential. With  $U = h(V_s)$ , the NDC model can correctly show the influence of the charge state on the terminal voltage, while inheriting all the capabilities of the original model.

Furthermore, the NDC model also contains an RC circuit,  $R_1-C_1$ , which, together with  $R_0$ , simulates the impedance-based part of the voltage dynamics. Here,  $R_0$  characterizes the linear kinetic aspect of the impedance, which relates to the ohmic resistance and solid electrolyte interface (SEI) resistance [55];  $R_1-C_1$  accounts for the voltage transients related with the charge transfer on the electrode/electrolyte interface and the ion mass diffusion in the electrodes [56]. This work finds that one RC circuit can offer sufficient fidelity, though it is possible to connect more RC circuits serially with  $R_1-C_1$  to gain better accuracy.

The dynamics of the NDC model can be expressed in the state-space form as follows:

$$\begin{cases} \begin{bmatrix} \dot{V}_b(t) \\ \dot{V}_s(t) \\ \dot{V}_1(t) \end{bmatrix} = A \begin{bmatrix} V_b(t) \\ V_s(t) \\ V_1(t) \end{bmatrix} + BI(t), & (1a) \\ V(t) = h(V_s(t)) - V_1(t) + R_0 I(t), & (1b) \end{cases}$$

where

$$A = \begin{bmatrix} \frac{-1}{C_b(R_b+R_s)} & \frac{1}{C_b(R_b+R_s)} & 0 \\ \frac{1}{C_s(R_b+R_s)} & \frac{-1}{C_s(R_b+R_s)} & 0 \\ 0 & 0 & \frac{-1}{R_1C_1} \end{bmatrix}, \quad B = \begin{bmatrix} \frac{R_s}{C_b(R_b+R_s)} \\ \frac{R_b}{C_s(R_b+R_s)} \\ \frac{-1}{C_1} \end{bmatrix}.$$

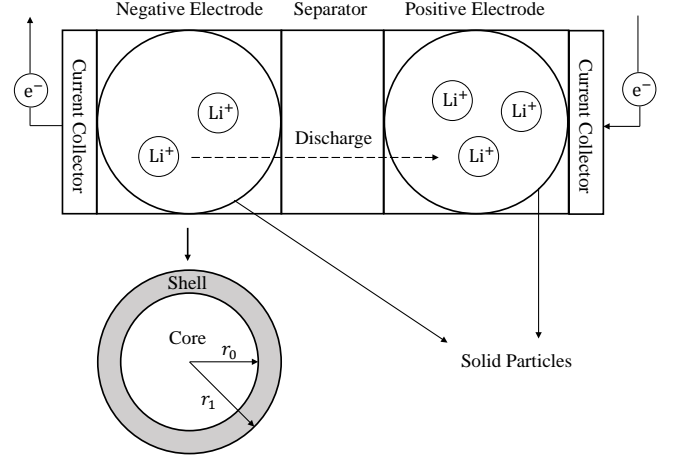


Figure 2: The single-particle model (top), and a particle (bottom) subdivided into two volumes, core and shell, which correspond to  $R_b-C_b$  and  $R_s-C_s$ , respectively.

In above,  $I > 0$  for charging,  $I < 0$  for discharging, and  $V_1$  refers to the voltage across the  $R_1-C_1$  circuit. One can parameterize  $h(V_s)$  as a polynomial. A fifth-order polynomial is empirically selected here:

$$h(V_s) = \alpha_0 + \alpha_1 V_s + \alpha_2 V_s^2 + \alpha_3 V_s^3 + \alpha_4 V_s^4 + \alpha_5 V_s^5,$$

where  $\alpha_i$  for  $i = 0, 1, \dots, 5$  are coefficients.

Note that  $V_b$  and  $V_s$  must be set to belong to an interval  $[\underline{V}_s, \overline{V}_s]$ . It is without loss of generality to let  $\underline{V}_s = 0$  V and  $\overline{V}_s = 1$  V. This implies that  $V_b = V_s = 1$  V at full charge (SoC = 100%) and that  $V_b = V_s = 0$  V for full depletion (SoC = 0%). Further, the SoC is given by

$$\text{SoC} = \frac{Q_a}{Q_t} = \frac{C_b V_b + C_s V_s}{C_b + C_s} \times 100\%, \quad (2)$$

where  $Q_t$  denotes the total capacity, i.e.,  $Q_t = C_b + C_s$ , and  $Q_a$  the available capacity, i.e.,  $Q_a = C_b V_b + C_s V_s$ , respectively. Meanwhile, it is worth noting that the SoC-OCV function in this setting shares the same form with  $h(\cdot)$ , i.e.,  $\text{OCV} = h(\text{SoC})$ . To see this point, recall that the OCV at every SoC refers to a cell's equilibrium voltage when there is no current load. Viewing (1b), one can see that the equilibrium voltage is exactly equal to  $h(V_s)$  because the voltage across  $R_0$  and  $R_1-C_1$  is zero then; when the cell is at equilibrium, it holds that  $\text{SoC} = V_b = V_s$  in terms of quantities, as (2) indicates. Hence, the SoC-OCV relation resembles that of  $U = h(V_s)$ . In addition, the internal resistance  $R_0$  is also assumed to be SoC-dependent following the recommendation in [57], taking the form of

$$R_0 = \gamma_1 + \gamma_2 e^{-\gamma_3 \text{SoC}} + \gamma_4 e^{-\gamma_5 (1-\text{SoC})}. \quad (3)$$

The rest of this paper will center on developing parameter identification approaches to determine the model parameters using measurement data and apply identified models to experimental datasets to evaluate their predictive accuracy.

### III. PARAMETER IDENTIFICATION 1.0: CONSTANT-CURRENT CHARGING/DISCHARGING

This section studies parameter identification for the NDC model when a constant current is applied to a battery. The discharging case is considered here without loss of generality. In a two-step procedure, the SoC-OCV relation is identified first, and then the impedance and capacitance parameters estimated next.

#### A. SoC-OCV Identification

The SoC-OCV curve of a battery can be obtained by discharging it using a small current (e.g., 1/25 C-rate as suggested in [29]) from full to empty. In this process, the terminal voltage  $V$  can be taken as the OCV. Immediately one can see that  $\alpha_0 = \underline{V}$  and  $\sum_{i=0}^5 \alpha_i = \bar{V}$ , where  $\underline{V}$  and  $\bar{V}$  are the minimum and maximum value of  $V$  in the process. Therefore, OCV =  $h(\text{SoC})$  can be written as a function of  $\alpha_i$  for  $i = 1, 2, \dots, 4$  as follows:

$$\text{OCV} = \underline{V} + \sum_{i=1}^4 \alpha_i \text{SoC}^i + \left( \bar{V} - \underline{V} - \sum_{i=1}^4 \alpha_i \right) \text{SoC}^5,$$

where OCV can be read directly from the terminal voltage measurements, and the corresponding SoC can be calculated using the coulomb counting method, i.e.,

$$\text{SoC} = \frac{Q_t + It}{Q_t} \times 100\%.$$

From above, one can observe that  $\alpha_i$  for  $i = 1, 2, \dots, 4$  can be identified by solving a data fitting problem, which can be addressed as a linear least squares problem. The identification results are unique and can be easily obtained. Then with  $\alpha_0 = \underline{V}$  and  $\alpha_5 = \bar{V} - \underline{V} - \sum_{i=1}^4 \alpha_i$ , the function  $h(\cdot)$  becomes explicit and ready for use.

#### B. Impedance and Capacitance Identification

Now, consider discharging the battery by a constant current of normal magnitude to determine the impedance and capacitance parameters. The identification can be attained by expressing the terminal voltage in terms of the parameters and then fitting it to the measurement data.

1) *Terminal Voltage Response Analysis*: Consider a battery left idling for a long period of time, and then discharge it using a constant current. According to (1a),  $V_s$  can be derived as

$$V_s(t) = V_s(0) + \frac{It}{C_b + C_s} + \frac{C_b(R_b C_b - R_s C_s)I}{(C_b + C_s)^2} \cdot \left[ 1 - \exp\left(-\frac{C_b + C_s}{C_b C_s (R_b + R_s)} t\right) \right], \quad (4)$$

where  $V_s(0)$  is known to us as it can be accessed from SoC(0) when the battery is initially relaxed. However, it is impossible to identify  $C_b$ ,  $R_b$ ,  $C_s$  and  $R_s$  altogether. This issue can be seen from (4), where  $V_s$  depends on three parameters, i.e.,  $1/(C_b + C_s)$ ,  $C_b(R_b C_b - R_s C_s)/(C_b + C_s)^2$  and  $(C_b + C_s)/[C_b C_s (R_b + R_s)]$ . Even if they are known, no one can extract all the four individual impedance and capacitance parameters from them. Therefore, it is sensible

to avoid the parameter redundancy by assuming  $R_s = 0$ , as recommended in [58]. This is a tenable assumption since  $R_s \ll R_b$  for the NDC model. As a result, (4) reduces to

$$V_s(t) = V_s(0) + \beta_1 It + \beta_2 I (1 - e^{-\beta_3 t}), \quad (5)$$

where

$$\beta_1 = \frac{1}{C_b + C_s}, \quad \beta_2 = \frac{R_b C_b^2}{(C_b + C_s)^2}, \quad \beta_3 = \frac{C_b + C_s}{C_b C_s R_b}.$$

Here,  $\beta_1$  is known because  $Q_t$  has been calibrated by coulomb counting in Section III-A. When  $\beta_2$  and  $\beta_3$  are also available,  $C_b$ ,  $C_s$  and  $R_b$  can be reconstructed as follows:

$$C_b = \frac{\beta_2 \beta_3}{\beta_1 (\beta_1 + \beta_2 \beta_3)}, \quad C_s = \frac{1}{\beta_1 + \beta_2 \beta_3}, \quad R_b = \frac{1}{\beta_1 \beta_3 C_b C_s}.$$

Further, in the above constant-current discharging scenario, the evolution of  $V_1$  follows

$$V_1(t) = V_1(0) - I\beta_4 (1 - e^{-\beta_5 t}), \quad (6)$$

where

$$\beta_4 = R_1, \quad \beta_5 = \frac{1}{R_1 C_1}.$$

Since the battery has idled for a long period prior to discharging,  $V_1(0)$  relaxes at zero and can be removed from (6).

Then, combining (1b), (3), (5) and (6), the terminal voltage response is given by

$$V(\theta; t) = \sum_{i=0}^5 \alpha_i V_s^i(\theta; t) + I\theta_3 (1 - e^{-\theta_4 t}) + I\theta_5 + I\theta_6 e^{-\theta_7 \text{SoC}(t)} + I\theta_8 e^{-\theta_9 (1 - \text{SoC}(t))}. \quad (7)$$

with

$$\theta = [\beta_2 \quad \beta_3 \quad \beta_4 \quad \beta_5 \quad \gamma_1 \quad \gamma_2 \quad \gamma_3 \quad \gamma_4 \quad \gamma_5]^\top,$$

and

$$V_s(\theta; t) = V_s(0) + It/Q_t + \theta_1 I (1 - e^{-\theta_2 t}), \\ \text{SoC}(t) = \text{SoC}(0) + It/Q_t.$$

2) *Data-Fitting-Based Identification of  $\theta$* : In above, the terminal voltage  $V$  is expressed in terms of  $\theta$ , allowing one to identify  $\theta$  by minimizing the difference between the measured voltage and the voltage predicted by (7). Hence, a data fitting problem similar to the one in Section III-A can be formulated. A caution yet is that the resultant optimization will be nonlinear and nonconvex due to the presence of  $h(\cdot)$ . As a consequence, a numerical algorithm may get stuck in local minima and eventually give unreasonable estimates. A promising way of mitigating this challenge is to constrain the numerical optimization search within a parameter space that is believably correct. Specifically, one can roughly determine the lower and upper bounds of part or all of the parameters, set up a limited search space, and run numerical optimization within this space. With this notion, the identification problem can be formulated as a constrained optimization problem:

$$\hat{\theta} = \arg \min_{\theta} \frac{1}{2} [\mathbf{y} - \mathbf{V}(\theta)]^\top \mathbf{Q}^{-1} [\mathbf{y} - \mathbf{V}(\theta)], \quad (8a)$$

$$\text{s.t. } \underline{\theta} \leq \theta \leq \bar{\theta}, \quad (8b)$$

where  $\hat{\theta}$  is the estimate of  $\theta$ ,  $\underline{\theta}$  and  $\bar{\theta}$  are the pre-set lower and upper bounds of  $\theta$ , respectively,  $\mathbf{y}$  the terminal voltage measurement vector,  $\mathbf{Q}$  an  $M \times M$  symmetric positive definite matrix representing the covariance of the measurement noise, with  $M$  being the number of the data points, and

$$\mathbf{y} = [y(t_1) \quad y(t_2) \quad \cdots \quad y(t_M)]^\top,$$

$$\mathbf{V}(\theta) = [V(\theta; t_1) \quad V(\theta; t_2) \quad \cdots \quad V(\theta; t_M)]^\top.$$

Multiple numerical algorithms are available in the literature to solve (8), a choice among which is the interior-point-based trust-region method [38].

#### IV. PARAMETER IDENTIFICATION 2.0: VARIABLE-CURRENT CHARGING/DISCHARGING

While it is not unusual to charge or discharge a battery at a constant current, real-world battery systems such as those in electric vehicles generally operate at variable currents. Motivated by practical utility, an interesting and challenging question is: Will it be possible to estimate all the parameters of the NDC model in one shot when an arbitrary current profile is applied to a battery? Having this question addressed will greatly improve the availability of the model, even to an on-demand level, for battery management tasks. This section offers a study in this regard from a Wiener identification perspective. It first unveils the NDC model's inherent Wiener-type structure and then develops an MAP-based identification approach. Here, the study assumes  $R_0$  to be constant for convenience.

##### A. Wiener-Type Structure of the NDC Model

The NDC model is structurally similar to a Wiener system—the double RC circuits constitute a linear dynamic subsystem, and cascaded with it is a nonlinear mapping. The following outlines the discrete-time Wiener-type formulation of (1).

Suppose that (1a) is sampled with a time period  $\Delta t$ . By applying the zero-order-hold discretization, the response of  $V_s$  in discrete-time domain is given by

$$V_s(t) = G_1(q)I(t) + G_2(q)V_s(0), \quad (9)$$

where  $q^{-1}$  is the backshift operator, and  $t$  is the discrete-time index, respectively. Consider a battery initially relaxed for a long time. In this regard,  $V_s(0) = \text{SoC}(0)$ , indicating that  $V_s(0)$  is known to us and thus free of identification. Furthermore,

$$G_1(q) = \frac{\beta_1 q^{-1} + \beta_2 q^{-2}}{1 - (1 + \beta_3)q^{-1} + \beta_3 q^{-2}},$$

$$G_2(q) = \frac{1}{1 - q^{-1}},$$

where

$$\beta_1 = \frac{A_{21}B_{11} + A_{12}B_{21}}{A_{12} + A_{21}} \Delta t$$

$$- \frac{A_{21}B_{11} - A_{21}B_{21}}{(A_{12} + A_{21})^2} (1 - \beta_3),$$

$$\beta_2 = -\frac{A_{21}B_{11} + A_{12}B_{21}}{A_{12} + A_{21}} \beta_3 \Delta t$$

$$+ \frac{A_{21}B_{11} - A_{21}B_{21}}{(A_{12} + A_{21})^2} (1 - \beta_3),$$

$$\beta_3 = e^{-(A_{12} + A_{21})\Delta t},$$

where the notation  $\beta$  is slightly abused without causing confusion. Notice that the same parameter redundancy issue as in Section III-B occurs here, because only three parameters,  $\beta_i$  for  $i = 1, 2, 3$ , appear in (9), though (1a) involves four physical parameters,  $C_b$ ,  $C_s$ ,  $R_b$  and  $R_s$ . To fix this, let  $R_s = 0$  as was done before. It then follows that

$$\beta_1 = \check{\beta}_1 + \check{\beta}_2,$$

$$\beta_2 = -\check{\beta}_1 \check{\beta}_3 - \check{\beta}_2,$$

$$\beta_3 = \check{\beta}_3,$$

with

$$\check{\beta}_1 = \frac{\Delta t}{C_b + C_s}, \quad \check{\beta}_2 = \frac{R_b C_b^2 (1 - \check{\beta}_3)}{(C_b + C_s)^2}, \quad \check{\beta}_3 = e^{-\frac{C_b + C_s}{C_b C_s R_b} \Delta t}.$$

Next, the response of  $V_1$  in discrete-time domain is given as follows

$$V_1(t) = G_3(q)I(t) + G_4(q)V_1(0), \quad (10)$$

where

$$G_3(q) = \frac{\beta_4 q^{-1}}{1 + \beta_5 q^{-1}}, \quad G_4(q) = \frac{1}{1 + \beta_5 q^{-1}},$$

with

$$\beta_4 = R_1 \left( e^{-\frac{\Delta t}{R_1 C_1}} - 1 \right), \quad \beta_5 = -e^{-\frac{\Delta t}{R_1 C_1}}.$$

Since  $V_1(0) = 0$  V for the initially relaxed battery,  $G_4(q)V_1(0)$  can be removed from (10) and is ignored in the following. If  $\check{\beta}_i$  for  $i = 1, 2, 3$ ,  $\beta_4$  and  $\beta_5$  are determined, the physical parameters can be reconstructed as follows:

$$C_b = \frac{\Delta t}{\check{\beta}_1} - C_s,$$

$$C_s = \frac{\check{\beta}_1 (1 - \check{\beta}_3) \Delta t}{\check{\beta}_1 (\check{\beta}_1 - \check{\beta}_1 \check{\beta}_3 - \check{\beta}_2 \log \check{\beta}_3)},$$

$$R_b = -\frac{(\Delta t)^2}{C_b C_s \check{\beta}_1 \log \check{\beta}_3},$$

$$R_1 = -\frac{\beta_4}{\beta_5 + 1},$$

$$C_1 = -\frac{\Delta t}{\log(-\beta_5) R_1}.$$

Finally, it is obvious that

$$V(t) = h [G_1(q)I(t) + G_2(q)V_s(0)] - G_3(q)I(t) + R_0 I(t). \quad (11)$$

The above equation reveals the block-oriented Wiener-type structure of the NDC model, as depicted in Figure 3, in which

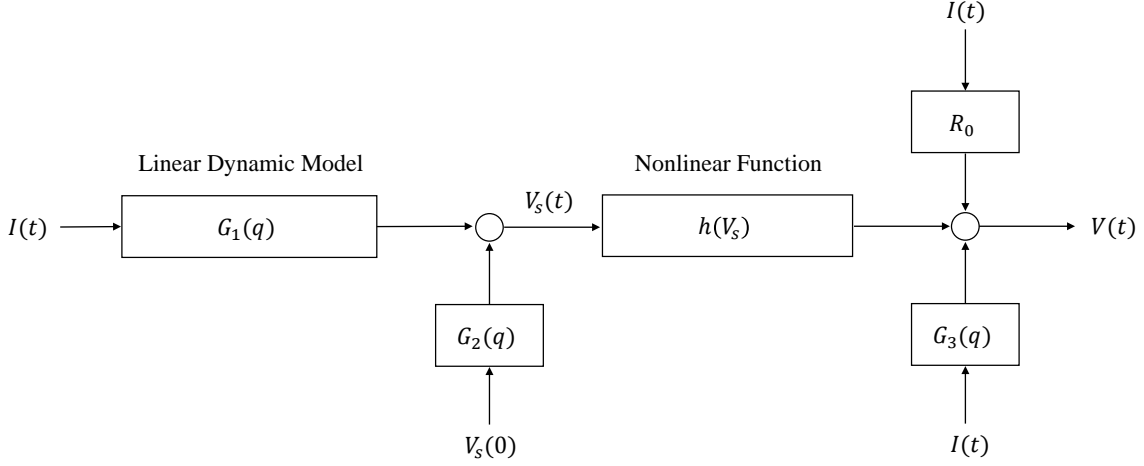


Figure 3: The Wiener-type structure of the nonlinear double-capacitor (NDC) model.

the linear dynamic model  $G_1(q)$  and the nonlinear function  $h(V_s)$  are interconnected sequentially. Given (11), the next pursuit is to estimate all of the parameters simultaneously, which include  $\alpha_i$  for  $i = 1, 2, \dots, 4$ ,  $\check{\beta}_i$  for  $i = 1, 2, 3$ ,  $\beta_4$ ,  $\beta_5$  and  $R_0$ . Here,  $\alpha_0$  and  $\alpha_5$  are free of identification as they can be expressed by  $\alpha_i$  for  $i = 1, 2, \dots, 4$  (see Section III-A). It is worth mentioning that this identification approach can also be applied to other ECMs like the Rint model [10] and the Thevenin model [38], as they can also be formulated as a cascaded Wiener-type structure similar to the one in Figure 3.

### B. MAP-Based Wiener Identification

Consider the following model based on (11) for notational convenience:

$$z(t) = V(\boldsymbol{\theta}; u(t)) + v(t), \quad (12)$$

where  $u$  is the input current  $I$ ,  $z$  the measured voltage,  $v$  the measurement noise added to  $V$  and assumed to follow a Gaussian distribution  $\mathcal{N}(0, \sigma^2)$ , and

$$\begin{aligned} & V(\boldsymbol{\theta}; u(t)) \\ &= h[G_1(q, \boldsymbol{\theta})u(t) + G_2(q)V_s(0), \boldsymbol{\theta}] - G_3(q, \boldsymbol{\theta})u(t) + \theta_{10}u(t), \end{aligned}$$

with

$$\boldsymbol{\theta} = [\alpha_1 \quad \alpha_2 \quad \alpha_3 \quad \alpha_4 \quad \check{\beta}_1 \quad \check{\beta}_2 \quad \check{\beta}_3 \quad \beta_4 \quad \beta_5 \quad R_0]^\top.$$

The input and output datasets are denoted as

$$\begin{aligned} \mathbf{u} &= [u(t_1) \quad u(t_2) \quad \dots \quad u(t_N)]^\top \in \mathbb{R}^{N \times 1}, \\ \mathbf{z} &= [z(t_1) \quad z(t_2) \quad \dots \quad z(t_N)]^\top \in \mathbb{R}^{N \times 1}, \end{aligned}$$

where  $N$  is the total number of data samples. A combination of them is expressed as

$$\mathbf{Z} = [\mathbf{u} \quad \mathbf{z}].$$

An ML-based approach is developed in [52] to deal with Wiener system identification. If applied to (12), it leads to consideration of the following problem:

$$\hat{\boldsymbol{\theta}} = \arg \max_{\boldsymbol{\theta}} p(\mathbf{Z}|\boldsymbol{\theta}).$$

Following this line, one can derive a likelihood cost function and perform minimization to find out  $\hat{\boldsymbol{\theta}}$ . However, this method can be vulnerable to the risk of local minima because of the nonconvexity issue resulting from the static nonlinear function  $h(\cdot)$ . This can cause unphysical estimates. While carefully selecting an initial guess is suggested to alleviate this problem [59], it is often found inadequate for many practical systems. In particular, our study showed that it could hardly deliver reliable parameter estimation when used to handle the NDC model identification.

MAP-based Wiener identification thus is proposed here to overcome this problem. The MAP estimation can incorporate some prior knowledge about parameters to help drive the parameter search toward a reasonable minimum point. Specifically, consider maximizing the *a posteriori* probability distribution of  $\boldsymbol{\theta}$  conditioned on  $\mathbf{Z}$ :

$$\hat{\boldsymbol{\theta}} = \arg \max_{\boldsymbol{\theta}} p(\boldsymbol{\theta}|\mathbf{Z}). \quad (13)$$

By the Bayes' theorem, it follows that

$$p(\boldsymbol{\theta}|\mathbf{Z}) = \frac{p(\mathbf{Z}|\boldsymbol{\theta}) \cdot p(\boldsymbol{\theta})}{p(\mathbf{Z})} \propto p(\mathbf{Z}|\boldsymbol{\theta}) \cdot p(\boldsymbol{\theta}).$$

In above,  $p(\boldsymbol{\theta})$  quantifies the prior information available about  $\boldsymbol{\theta}$ . A general way is to characterize it as a Gaussian random vector following the distribution  $p(\boldsymbol{\theta}) \sim \mathcal{N}(\mathbf{m}, \mathbf{P})$ . Based on (12),  $p(\mathbf{z}|\boldsymbol{\theta}) \sim \mathcal{N}(\mathbf{V}(\boldsymbol{\theta}; \mathbf{u}), \mathbf{R})$ , where  $\mathbf{R} = \sigma^2 \mathbf{I}$  and

$$\mathbf{V}(\boldsymbol{\theta}; \mathbf{u}) = [V(\boldsymbol{\theta}; u(t_1)) \quad \dots \quad V(\boldsymbol{\theta}; u(t_N))]^\top.$$

Then,

$$\begin{aligned} & p(\mathbf{Z}|\boldsymbol{\theta}) \cdot p(\boldsymbol{\theta}) \\ & \propto \exp\left(-\frac{1}{2}[\mathbf{z} - \mathbf{V}(\boldsymbol{\theta}; \mathbf{u})]^\top \mathbf{R}^{-1}[\mathbf{z} - \mathbf{V}(\boldsymbol{\theta}; \mathbf{u})]\right) \\ & \quad \cdot \exp\left(-\frac{1}{2}(\boldsymbol{\theta} - \mathbf{m})^\top \mathbf{P}^{-1}(\boldsymbol{\theta} - \mathbf{m})\right). \end{aligned}$$

If using the log-likelihood, the problem in (13) is equivalent to

$$\hat{\boldsymbol{\theta}} = \arg \min_{\boldsymbol{\theta}} J(\boldsymbol{\theta}), \quad (14)$$

where

$$J(\boldsymbol{\theta}) = \frac{1}{2} [\mathbf{z} - \mathbf{V}(\boldsymbol{\theta}; \mathbf{u})]^\top \mathbf{R}^{-1} [\mathbf{z} - \mathbf{V}(\boldsymbol{\theta}; \mathbf{u})] + \frac{1}{2} (\boldsymbol{\theta} - \mathbf{m})^\top \mathbf{P}^{-1} (\boldsymbol{\theta} - \mathbf{m}).$$

The quasi-Newton method can be exploited to numerically solve the nonlinear optimization problem in (14) [52]. This method iteratively updates the parameter estimate through

$$\boldsymbol{\theta}_{k+1} = \boldsymbol{\theta}_k + \lambda_k \mathbf{s}_k. \quad (15)$$

Here,  $\lambda_k$  denotes the step size at iteration step  $k$ , and  $\mathbf{s}_k$  is the gradient-based search direction given by

$$\mathbf{s}_k = -\mathbf{B}_k \mathbf{g}_k, \quad (16)$$

where  $\mathbf{B}_k \in \mathbb{R}^{8 \times 8}$  is a positive definite matrix that approximates the Hessian matrix  $\nabla^2 J(\boldsymbol{\theta}_k)$ , and  $\mathbf{g}_k = \nabla J(\boldsymbol{\theta}_k) \in \mathbb{R}^{8 \times 1}$ . Based on the well-known BFGS update strategy [60],  $\mathbf{B}_k$  can be updated by

$$\mathbf{B}_k = \left( \mathbf{I} - \frac{\boldsymbol{\delta}_k \boldsymbol{\gamma}_k^\top}{\boldsymbol{\delta}_k^\top \boldsymbol{\gamma}_k} \right) \mathbf{B}_{k-1} \left( \mathbf{I} - \frac{\boldsymbol{\gamma}_k \boldsymbol{\delta}_k^\top}{\boldsymbol{\delta}_k^\top \boldsymbol{\gamma}_k} \right) + \frac{\boldsymbol{\delta}_k \boldsymbol{\delta}_k^\top}{\boldsymbol{\delta}_k^\top \boldsymbol{\gamma}_k}, \quad (17)$$

with  $\boldsymbol{\delta}_k = \boldsymbol{\theta}_k - \boldsymbol{\theta}_{k-1}$  and  $\boldsymbol{\gamma}_k = \mathbf{g}_k - \mathbf{g}_{k-1}$ . In addition,

$$\mathbf{g}_k = - \left( \frac{\partial \mathbf{V}(\boldsymbol{\theta}_k; \mathbf{u})}{\partial \boldsymbol{\theta}_k} \right)^\top \mathbf{R}^{-1} [\mathbf{z} - \mathbf{V}(\boldsymbol{\theta}_k; \mathbf{u})] + \mathbf{P}^{-1} (\boldsymbol{\theta}_k - \mathbf{m}), \quad (18)$$

where each column of  $\frac{\partial \mathbf{V}(\boldsymbol{\theta}; \mathbf{u})}{\partial \boldsymbol{\theta}} \in \mathbb{R}^{N \times 8}$  is given by

$$\begin{aligned} \frac{\partial \mathbf{V}(\boldsymbol{\theta}; \mathbf{u})}{\partial \theta_i} &= \mathbf{x}^{\circ i} - \mathbf{x}^{\circ 5} \text{ for } i = 1, 2, \dots, 4, \\ \frac{\partial \mathbf{V}(\boldsymbol{\theta}; \mathbf{u})}{\partial \theta_5} &= \boldsymbol{\Sigma} \circ \frac{q^{-1} - \theta_7 q^{-2}}{1 - (1 + \theta_7)q^{-1} + \theta_7 q^{-2}} \mathbf{u}, \\ \frac{\partial \mathbf{V}(\boldsymbol{\theta}; \mathbf{u})}{\partial \theta_6} &= \boldsymbol{\Sigma} \circ \frac{q^{-1} - q^{-2}}{1 - (1 + \theta_7)q^{-1} + \theta_7 q^{-2}} \mathbf{u}, \\ \frac{\partial \mathbf{V}(\boldsymbol{\theta}; \mathbf{u})}{\partial \theta_7} &= \boldsymbol{\Sigma} \circ \frac{\theta_6 q^{-2} - 2\theta_6 q^{-3} + \theta_6 q^{-4}}{(1 - (1 + \theta_7)q^{-1} + \theta_7 q^{-2})^2} \mathbf{u}, \\ \frac{\partial \mathbf{V}(\boldsymbol{\theta}; \mathbf{u})}{\partial \theta_8} &= \frac{-q^{-1}}{1 + \theta_9 q^{-1}} \mathbf{u}, \\ \frac{\partial \mathbf{V}(\boldsymbol{\theta}; \mathbf{u})}{\partial \theta_9} &= \frac{\theta_8 q^{-2}}{1 + 2\theta_9 q^{-1} + \theta_9^2 q^{-2}} \mathbf{u}, \\ \frac{\partial \mathbf{V}(\boldsymbol{\theta}; \mathbf{u})}{\partial \theta_{10}} &= \mathbf{u}, \end{aligned}$$

with

$$\begin{aligned} \mathbf{x} &= G_1(q, \boldsymbol{\theta}) \mathbf{u} + G_2(q) V_s(0) \mathbf{1}, \\ \boldsymbol{\Sigma} &= \sum_{i=1}^4 i \theta_i \mathbf{x}^{\circ(i-1)} + 5 \left( \bar{V} - \underline{V} - \sum_{i=1}^4 \theta_i \right) \mathbf{x}^{\circ 4}. \end{aligned}$$

Here,  $\mathbf{x} \circ \mathbf{u}$  denotes the Hadamard product of  $\mathbf{x}$  and  $\mathbf{u}$ ,  $\mathbf{x}^{\circ 2}$  denotes the Hadamard power with  $\mathbf{x}^{\circ 2} = \mathbf{x} \circ \mathbf{x}$ , and  $\mathbf{1} \in \mathbb{R}^{N \times 1}$  denotes a column vector with all elements equal to one. Finally, note that  $\lambda_k$  needs to be chosen carefully to make  $J(\boldsymbol{\theta})$  decrease monotonically. One can use the Wolfe conditions and let  $\lambda_k$  be selected such that

$$J(\boldsymbol{\theta}_k + \lambda_k \mathbf{s}_k) \leq J(\boldsymbol{\theta}_k) + c_1 \lambda_k \mathbf{g}_k^\top \mathbf{s}_k, \quad (19a)$$

$$\nabla J(\boldsymbol{\theta}_k + \lambda_k \mathbf{s}_k)^\top \mathbf{s}_k \geq c_2 \nabla J(\boldsymbol{\theta}_k)^\top \mathbf{s}_k, \quad (19b)$$

Table I: Quasi-Newton-based implementation for MAP-based Wiener identification.

<p>Initialize <math>\boldsymbol{\theta}_0</math> and set the convergence tolerance</p> <p><b>repeat</b></p> <p>  Compute <math>\mathbf{g}_k</math> via (18)</p> <p>  <b>if</b> <math>k = 0</math> <b>then</b></p> <p>    Initialize <math>\mathbf{B}_0 = 0.001 \frac{1}{\ \mathbf{g}_0\ } \mathbf{I}</math></p> <p>  <b>else</b></p> <p>    Compute <math>\mathbf{B}_k</math> via (17)</p> <p>  <b>end if</b></p> <p>  Compute <math>\mathbf{s}_k</math> via (16)</p> <p>  Find <math>\lambda_k</math> that satisfies the Wolfe conditions (19)</p> <p>  Perform the update via (15)</p> <p><b>until</b> <math>J(\boldsymbol{\theta}_k)</math> converges</p> <p><b>return</b> <math>\hat{\boldsymbol{\theta}} = \boldsymbol{\theta}_k</math></p>
--

with  $0 < c_1 < c_2 < 1$ . For the quasi-Newton method,  $c_1$  is usually set to be quite small, e.g.,  $c_1 = 10^{-6}$ , and  $c_2$  is typically set to be 0.9. The selection of  $\lambda_k$  can be based on trial and error in implementation. One can start with picking a number and check the Wolfe conditions. If the conditions are not satisfied, reduce the number and check again. An interested reader is referred to [60] for detailed discussion about the  $\lambda_k$  selection. Summarizing the above, Table I outlines the implementation procedure for the MAP-based Wiener identification.

*Remark 2:* While the MAP estimation has enjoyed a long history of addressing a variety of estimation problems, no study has been reported about its application to Wiener system identification to our knowledge. Here, it is found to be a very useful approach for providing physically reasonable parameter estimation for practical systems, as it takes into account some prior knowledge about the unknown parameters. In a Gaussian setting as adopted here, the prior  $p(\boldsymbol{\theta})$  translates into a regularization term in  $J(\boldsymbol{\theta})$ , which prevents incorrect fitting and enhances the robustness of the numerical optimization against nonconvexity.

*Remark 3:* The proposed MAP-based identification approach requires some prior knowledge of the parameters to be available. One can develop such a prior knowledge in several ways in practice. First,  $R_0$  can be roughly estimated using the voltage drop at the beginning of the discharge, to which it is a main contributor. Second, the polynomial coefficients of  $h(\cdot)$  can be approximately obtained from an experimentally calibrated SoC-OCV curve if there is any. Third, one can derive a rough range for  $C_b + C_s$  if a battery's capacity is approximately known. Finally, as the parameters of batteries of the same kind and brand are usually close, one can take the parameter estimates acquired from one battery as prior knowledge for another.

*Remark 4:* It is noticed that some other ECMs, e.g., the Rint, Thevenin and DP models, also have a Wiener-like structure. Therefore, the notion of MAP-based Wiener identification can be readily extended to identify them. One can follow similar lines to develop the computational procedures for each, and hence the details are skipped here.



Figure 4: PEC<sup>®</sup> SBT4050 battery tester.

## V. EXPERIMENTAL VALIDATION

This section presents experimental validation of the proposed NDC model and parameter identification 1.0 and 2.0 approaches. All the experiments in this section were conducted on a PEC<sup>®</sup> SBT4050 battery tester, see Figure 4. It can support charging/discharging with arbitrary current-, voltage- and power-based loads (up to 40 V and 50 A). A specialized server is used to prepare and configure a test offline and collect experimental data online *via* the associated software LifeTest<sup>™</sup>. Using this facility, charging/discharging tests were performed to generate data on a Panasonic NCR18650B lithium-ion battery cell, which was set to operate between 3.2 V (fully discharged) and 4.2 V (fully charged).

### A. Validation Based on Parameter Identification 1.0

This validation first extracts the NDC model from training datasets using the 1.0 identification approach in Section III and then applies the identified model to validation datasets to assess its predictive capability.

As a first step, the cell was fully charged and relaxed for a long time period. Then, a full discharge test was applied to the cell using a trickle constant current of 0.1 A (about 1/30 C-rate). With this test, the total capacity is determined to be  $Q_t = 3.06$  Ah by coulomb counting, implying  $C_b + C_s = 11,011$  F. Further, the SoC-OCV relation is identified as

$$\begin{aligned} \text{OCV} = & 3.2 + 2.59 \cdot \text{SoC} - 9.003 \cdot \text{SoC}^2 + 18.87 \cdot \text{SoC}^3 \\ & - 17.82 \cdot \text{SoC}^4 + 6.325 \cdot \text{SoC}^5, \end{aligned}$$

which establishes  $h(\cdot)$  immediately. The measured and identified SoC-OCV curves are compared in Figure 5. Next, the cell was fully charged again and left idling for a long time. It then was fully discharged using a constant current of 3 A to produce data for estimation of the impedance and capacitance parameters. The identification was achieved by solving the constrained optimization problem in (8). Table II summarizes the initial guess, lower and upper bounds, and obtained estimates of the parameters. The physical parameter estimates are extracted as:  $C_b = 10,037$  F,  $C_s = 973$  F,  $R_b = 0.019$   $\Omega$ ,  $R_s = 0$ ,  $R_1 = 0.02$   $\Omega$ ,  $C_1 = 3,250$  F, and

$$R_0 = 0.0531 + 0.1077e^{-3.807 \cdot \text{SoC}} + 0.0533e^{-7.613 \cdot (1 - \text{SoC})}.$$

The model is now fully available through the above two steps. Figure 6 shows that it accurately fits with the measurement data.

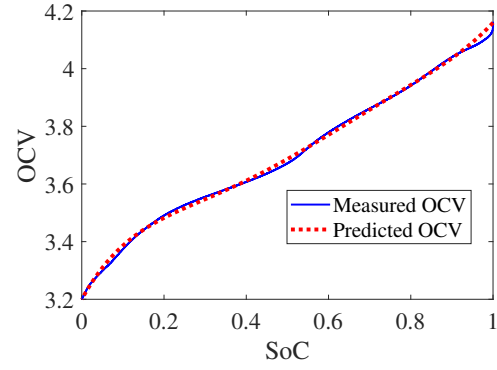


Figure 5: Identification 1.0: parameter identification of  $h(\cdot)$  that defines SoC-OCV relation.

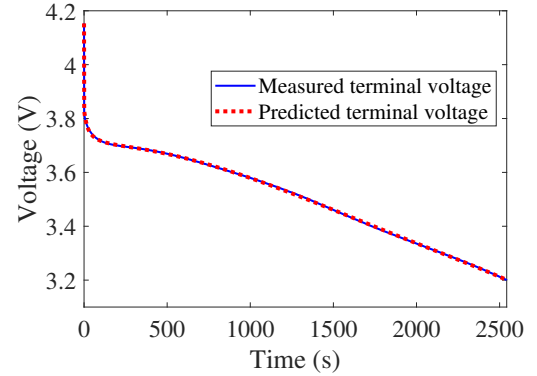


Figure 6: Identification 1.0: model fitting with the training data obtained under 3 A constant-current discharging.

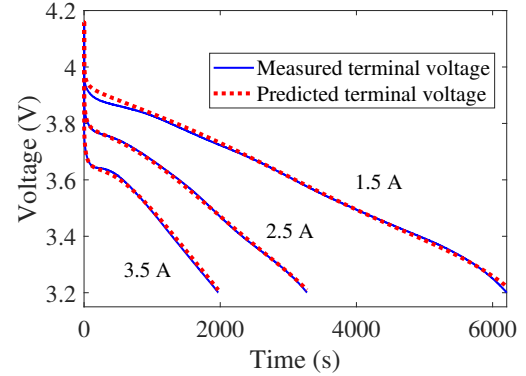


Figure 7: Identification 1.0: predictive fitting over validation data obtained by discharging at different constant currents.

As a model generally can well fit a training dataset, it is more meaningful and revealing to examine its predictive performance on some different datasets. Hence, five more tests were conducted by discharging the cell using constant currents of 1.5 A, 2.5 A and 3.5 A and two variable current profiles, respectively. Figure 7 shows that the identified model can predict the cell's voltage for discharging at constant currents at a high accuracy. The variable current profiles are portrayed in Figures 8(a) and 9(a), which were created by scaling the the Urban Dynamometer Driving Schedule (UDDS) profile in [61]

Table II: Identification 1.0: initial guess, bound limits and identification results.

Name	$\beta_2$	$\beta_3$	$\beta_4$	$\beta_5$	$\gamma_1$	$\gamma_2$	$\gamma_3$	$\gamma_4$	$\gamma_5$
Initial guess	0.02	0.05	0.005	1/100	0.05	0.2	8	0.07	12
$\underline{\theta}$	0.005	0.005	0.001	1/800	0.01	0.05	1	0.01	1
$\bar{\theta}$	0.2	0.2	0.03	1/10	0.09	0.35	15	0.12	15
$\hat{\theta}$	0.0163	0.0575	0.02	1/65	0.0531	0.1077	3.807	0.0533	7.613

Note: quantities are given in SI standard units in Tables II and III.

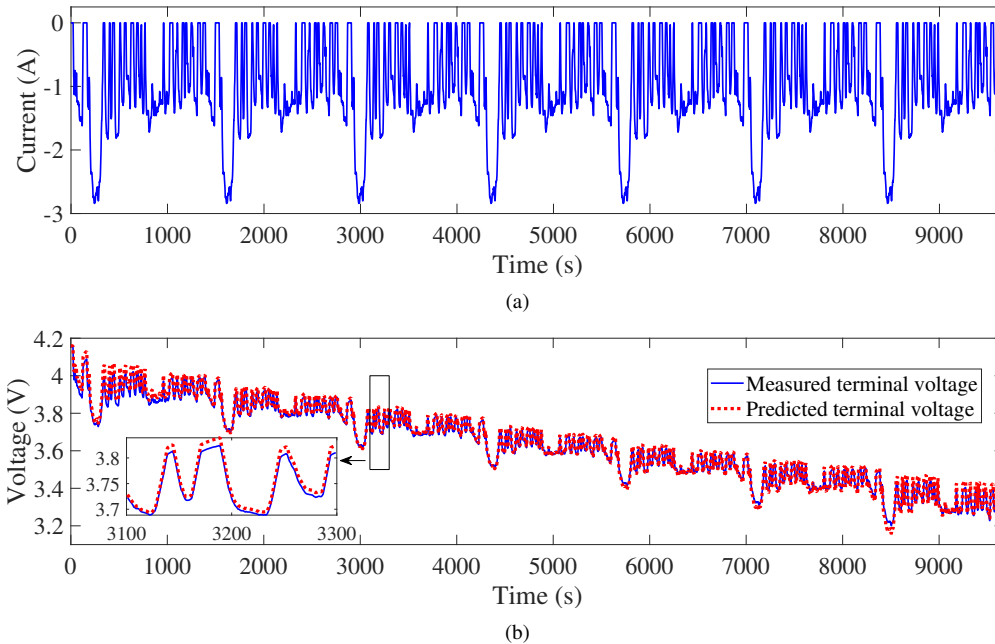


Figure 8: Identification 1.0: predictive fitting over validation data obtained by discharging at varying currents (0~3 A).

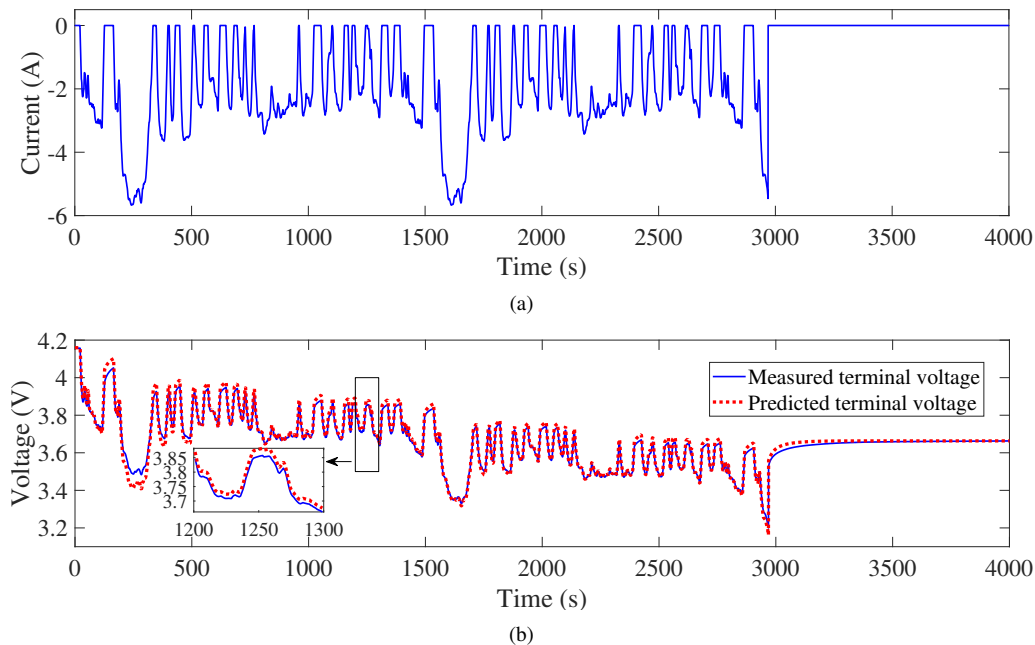


Figure 9: Identification 1.0: predictive fitting over validation dataset obtained by discharging at varying currents (0 ~ 6 A).

to span the ranges of 0~3 A and 0~6 A, respectively. Figures 8(b) and 9(b) present the predictive fitting results. Both of them illustrate that the model-based voltage prediction is quite close to the actual measurements. These results demonstrate

the excellent predictive capability of the NDC model.

### B. Validation Based on Parameter Identification 2.0

Let us now consider the 2.0 identification approach developed in Section III, which treats the NDC model as a Wiener-type system and performs MAP-based parameter estimation. This approach advantageously allows all the parameters to be estimated in a convenient one-shot procedure.

Following the manner in Section V-A, one can apply the 2.0 identification approach to a training dataset to extract an NDC model and then use it to predict the responses over several other different datasets. The validation here is also set to evaluate the NDC model against the Rint model [10] and the Thevenin model with one serial RC circuit [10], which are commonly used in the literature. The comparison also extends to a basic version of the NDC model (referred to as “basic NDC” in sequel), one with a constant  $R_0$  and without  $R_1$ - $C_1$  circuit, with the purpose of examining the utility of the NDC model when it is reduced to a simpler form. From the perspective of model structure, the NDC and Thevenin models belong to the same category, and the basic NDC and Rint models to another.

These four models are all Wiener-type, so the 2.0 identification approach can be used to identify them on the same training dataset, i.e., the one shown in Figure 8, thus ensuring a fair comparison. Table III summarizes the parameter setting and estimation for the NDC model. The resultant physical parameter estimates are given by:  $C_b = 10,031$  F,  $C_s = 979$  F,  $R_b = 0.063$   $\Omega$ ,  $R_s = 0$ ,  $R_1 = 0.002$   $\Omega$ ,  $C_1 = 2,449$  F and  $R_0 = 0.069$   $\Omega$ . The identification results for the the Rint, Thevenin model and basic NDC models are omitted here for the sake of space.

Figure 10(a) depicts how the identified models fit with the training dataset. One can observe that the NDC model and its basic version show excellent fitting accuracy, overall better than the Rint and Thevenin models. A more detailed comparison is given in Figure 10(b), which displays the fitting error in percentage. It is seen that the Rint model shows the least accuracy, followed by the Thevenin model. The NDC model and its basic version well outperform them, with the NDC model performing slightly even better.

Proceeding forward, let us investigate the predictive performance of the four models over several validation datasets. First, consider the datasets obtained by constant-current discharging at 1.5 A, 2.5 A and 3.5 A, as illustrated in Figure 7. Figure 11 demonstrates that the NDC model and its basic version can predict the voltage responses under different currents much more accurately than the Rint and Thevenin models. Next, consider the dataset in Figure 9 based on variable-current discharging. Figure 12 shows that the prediction accuracy of all the models is lower than the fitting accuracy, which is understandable. However, the NDC model and its basic version are still again the most capable of predicting, with the error mostly lying below 1%. As a contrast, while the Thevenin model can offer a decent fit with the training dataset as shown in Figure 10, its prediction accuracy over the validation dataset is not as satisfactory. This implies that it is less predictive than the NDC model.

Another evaluation of interest is about the SoC-OCV relation. As mentioned earlier, the 2.0 identification approach can estimate all the parameters, including the SoC-OCV function, in just one shot. Here, for the NDC model, the SoC-OCV function is identified as

$$\text{OCV} = 3.2 + 2.32 \cdot \text{SoC} - 8.15 \cdot \text{SoC}^2 + 19.345 \cdot \text{SoC}^3 - 20.78 \cdot \text{SoC}^4 + 8.222 \cdot \text{SoC}^5.$$

Identification of the other three models can also lead to estimation of this function. Figure 13 compares them with the benchmark shown in Figure 5, which is obtained experimentally by discharging the cell using a small current of 0.1 A. It is obvious that that the SoC-OCV curves obtained in the identification of the NDC model and its basic version are closer to the benchmark overall. This further shows the benefit of the NDC model as well as the efficacy of the 2.0 identification approach.

Summing up the above validation results, one can draw the following observations:

- The NDC model is the most competent among the four considered models for grasping and predicting a battery’s dynamic behavior, justifying its validity and soundness.
- The basic NDC model can offer fitting and prediction accuracy almost comparable to that of the full model. It thus can be well qualified if a practitioner wants to use a simpler NDC model yet without much loss of accuracy.
- The 2.0 identification approach is effective in estimating all the parameters of the NDC model as well as the Rint and Thevenin models in one shot from arbitrary data profiles. It can not only ease the cost of identification considerably but also provide on-demand model availability potentially in practice.

## VI. CONCLUSION

With the growing use and importance, real-time battery management has imposed a pressing demand for battery models with high fidelity and low complexity, making ECMs a popular choice in this field. The double-capacitor model is emerging as a favorable ECM for diverse applications, promising several advantages for capturing a battery’s dynamics. However, its linear structure intrinsically hinders a characterization of a battery’s nonlinear phenomena. To thoroughly improve this model, this paper proposed to modify its original structure by adding a nonlinear-mapping-based voltage source and a serial RC circuit. This development was justified through an analogous comparison with the SPM. Furthermore, two parameter estimation approaches, which were named 1.0 and 2.0, respectively, were designed to identify the model from current/voltage data. The 1.0 approach considers the constant-current charging/discharging scenarios, determining the SoC-OCV relation first and then estimating the impedance and capacitance parameters. With the observation that the NDC model has a Wiener-type structure, the 2.0 approach was derived from the Wiener perspective. As the first of its kind, it leverages the notion of MAP to address the issue of local minima that may reduce or damage the performance of the nonlinear Wiener system identification. It well lends itself

Table III: Identification 2.0: Initial guess, prior knowledge and identification results.

Name	$\alpha_1$	$\alpha_2$	$\alpha_3$	$\alpha_4$	$\check{\beta}_1$	$\check{\beta}_2$	$\check{\beta}_3$	$\beta_4$	$\beta_5$	$R_0$
Initial guess	2.59	-9.003	18.87	-17.82	$9.078 \times 10^{-5}$	$8.914 \times 10^{-4}$	0.964	$-4.938 \times 10^{-4}$	-0.9753	0.08
$m$	-	-	-	-	$9.078 \times 10^{-5}$	$8.914 \times 10^{-4}$	0.964	$-4.938 \times 10^{-4}$	-0.9753	0.08
$\sqrt{\text{diag}(\mathbf{P})}$	-	-	-	-	$0.001 \times m_5$	$0.15 \times m_6$	$0.15 \times m_7$	$0.15 \times m_8$	$0.15 \times m_9$	$0.15 \times m_{10}$
$\hat{\theta}$	2.32	-8.15	19.345	-20.78	$9.082 \times 10^{-5}$	$9.227 \times 10^{-4}$	0.982	$-4.859 \times 10^{-4}$	-0.8153	0.069

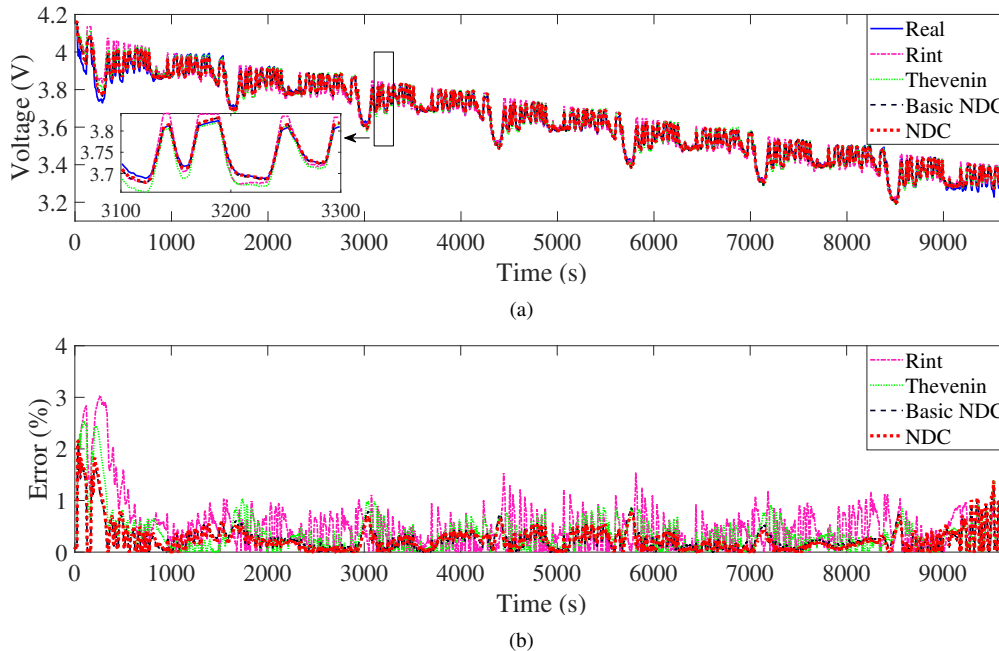


Figure 10: Identification 2.0: (a) model fitting with training data; (b) fitting error in percentage.

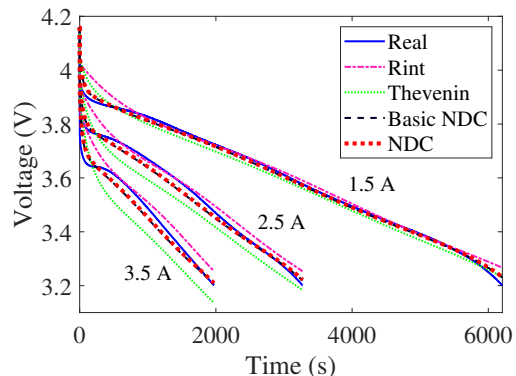


Figure 11: Identification 2.0: predictive fitting over validation dataset obtained by discharging at different varying currents.

to the variable-current charging/discharging scenarios and can desirably estimate all the parameters in one shot. The experimental evaluation demonstrated that the NDC model was more competitive than the popularly used Rint and Thevenin models in predicting a battery's behavior, in addition to showing the effectiveness of the identification approaches for extracting parameters. The future work will include enhancing the NDC model further to include the voltage hysteresis and temperature dynamics and building new battery estimation and control

design based on this model.

## REFERENCES

- [1] V. H. Johnson and A. A. Pesaran, "Temperature-dependent battery models for high-power lithium-ion batteries," National Renewable Energy Laboratory, Tech. Rep. NREL/CP-540-28716, 2000.
- [2] M. Doyle, T. F. Fuller, and J. Newman, "Modeling of galvanostatic charge and discharge of the lithium/polymer/insertion cell," *Journal of The Electrochemical Society*, vol. 140, no. 6, pp. 1526–1533, 1993.
- [3] J. C. Forman, S. J. Moura, J. L. Stein, and H. K. Fathy, "Genetic identification and fisher identifiability analysis of the Doyle–Fuller–Newman model from experimental cycling of a LiFePO<sub>4</sub> cell," *Journal of Power Sources*, vol. 210, pp. 263 – 275, 2012.
- [4] N. Chaturvedi, R. Klein, J. Christensen, J. Ahmed, and A. Kojic, "Algorithms for advanced battery-management systems," *IEEE Control Systems Magazine*, vol. 30, no. 3, pp. 49–68, 2010.
- [5] M. Guo, G. Sikha, and R. E. White, "Single-particle model for a lithium-ion cell: Thermal behavior," *Journal of The Electrochemical Society*, vol. 158, no. 2, pp. A122–A132, 2011.
- [6] C. Zou, C. Manzie, and D. Nešić, "A framework for simplification of PDE-based lithium-ion battery models," *IEEE Transactions on Control Systems Technology*, vol. 24, no. 5, pp. 1594–1609, 2016.
- [7] J. E. B. Randles, "Kinetics of rapid electrode reactions," *Discussions of the Faraday Society*, vol. 1, pp. 11–19, 1947.
- [8] A. I. Zia and S. C. Mukhopadhyay, *Impedance Spectroscopy and Experimental Setup*. Springer International Publishing, 2016, pp. 21–37.
- [9] S. M. G. and M. Nikdel, "Various battery models for various simulation studies and applications," *Renewable and Sustainable Energy Reviews*, vol. 32, pp. 477–485, 2014.
- [10] H. He, R. Xiong, and J. Fan, "Evaluation of lithium-ion battery equivalent circuit models for state of charge estimation by an experimental approach," *Energies*, vol. 4, pp. 582–598, 2011.

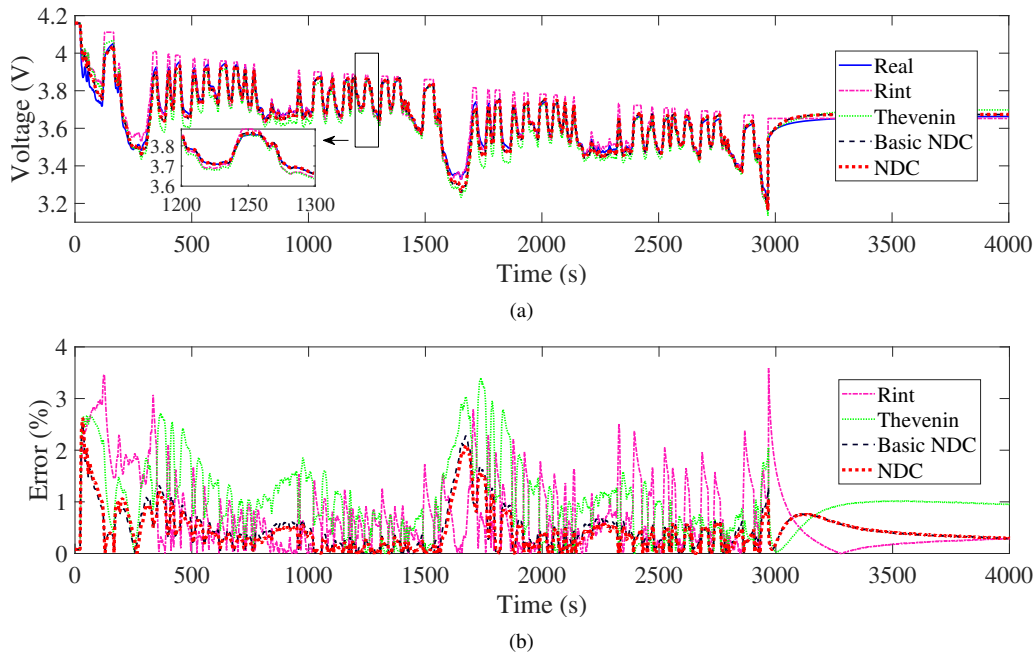


Figure 12: Identification 2.0: (a) predictive fitting over validation dataset obtained by discharging at varying currents between 0 A and 6 A; (b) predictive fitting error in percentage.

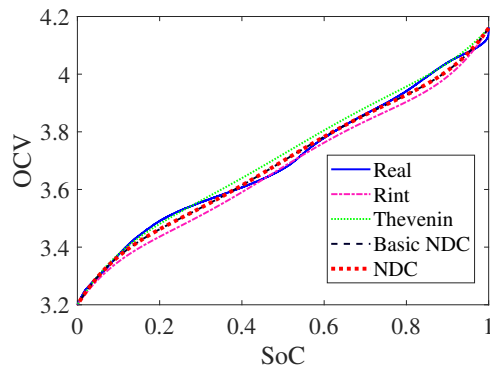


Figure 13: Identification 2.0: identification of the SoC-OCV relation based on different models, compared to the truth.

- [11] G. L. Plett, *Battery Management Systems, Volume 1: Battery Modeling*. Artech House, 2015.
- [12] C. Weng, J. Sun, and H. Peng, "A unified open-circuit-voltage model of lithium-ion batteries for state-of-charge estimation and state-of-health monitoring," *Journal of Power Sources*, vol. 258, pp. 228–237, 2014.
- [13] X. Lin, H. E. Perez, S. Mohan, J. B. Siegel, A. G. Stefanopoulou, Y. Ding, and M. P. Castanier, "A lumped-parameter electro-thermal model for cylindrical batteries," *Journal of Power Sources*, vol. 257, pp. 1–11, 2014.
- [14] M. Gholizadeh and F. R. Salmasi, "Estimation of state of charge, unknown nonlinearities, and state of health of a lithium-ion battery based on a comprehensive unobservable model," *IEEE Transactions on Industrial Electronics*, vol. 61, no. 3, pp. 1335–1344, 2014.
- [15] H. E. Perez, X. Hu, S. Dey, and S. J. Moura, "Optimal charging of Li-ion batteries with coupled electro-thermal-aging dynamics," *IEEE Transactions on Vehicular Technology*, vol. 66, no. 9, pp. 7761–7770, 2017.
- [16] Y. Wang, H. Fang, L. Zhou, and T. Wada, "Revisiting the state-of-charge estimation for lithium-ion batteries: A methodical investigation of the extended Kalman filter approach," *IEEE Control Systems*, vol. 37, no. 4, pp. 73–96, 2017.
- [17] G. L. Plett, "Extended Kalman filtering for battery management systems of LiPB-based HEV battery packs: Part 2. Modeling and identification," *Journal of Power Sources*, vol. 134, no. 2, pp. 262–276, 2004.
- [18] X. Hu, S. Li, and H. Peng, "A comparative study of equivalent circuit models for Li-ion batteries," *Journal of Power Sources*, vol. 198, pp. 359–367, 2012.
- [19] K. Li, F. Wei, K. J. Tseng, and B.-H. Soong, "A practical lithium-ion battery model for state of energy and voltage responses prediction incorporating temperature and ageing effects," *IEEE Transactions on Industrial Electronics*, vol. 65, no. 8, pp. 6696–6708, 2018.
- [20] K.-T. Lee, M.-J. Dai, and C.-C. Chuang, "Temperature-compensated model for lithium-ion polymer batteries with extended Kalman filter state-of-charge estimation for an implantable charger," *IEEE Transactions on Industrial Electronics*, vol. 65, no. 1, pp. 589–596, 2018.
- [21] M. Chen and G. A. Rincon-Mora, "Accurate electrical battery model capable of predicting runtime and I-V performance," *IEEE Transactions on Energy Conversion*, vol. 21, no. 2, pp. 504–511, 2006.
- [22] T. Kim and W. Qiao, "A hybrid battery model capable of capturing dynamic circuit characteristics and nonlinear capacity effects," *IEEE Transactions on Energy Conversion*, vol. 26, no. 4, pp. 1172–1180, 2011.
- [23] V. Johnson, "Battery performance models in ADVISOR," *Journal of Power Sources*, vol. 110, no. 2, pp. 321–329, 2002.
- [24] H. Fang, Y. Wang, and J. Chen, "Health-aware and user-involved battery charging management for electric vehicles: Linear quadratic strategies," *IEEE Transactions on Control Systems Technology*, vol. 25, no. 3, pp. 911–923, 2017.
- [25] H. Fang, C. Depcik, and V. Lvovich, "Optimal pulse-modulated lithium-ion battery charging: Algorithms and simulation," *Journal of Energy Storage*, vol. 15, pp. 359–367, 2018.
- [26] B. Schweighofer, K. M. Raab, and G. Brasseur, "Modeling of high power automotive batteries by the use of an automated test system," *IEEE Transactions on Instrumentation and Measurement*, vol. 52, no. 4, pp. 1087–1091, 2003.
- [27] S. Abu-Sharkh and D. Doerffel, "Rapid test and non-linear model characterisation of solid-state lithium-ion batteries," *Journal of Power Sources*, vol. 130, no. 1, pp. 266–274, 2004.
- [28] A. Fairweather, M. Foster, and D. Stone, "Battery parameter identification with Pseudo Random Binary Sequence excitation (PRBS)," *Journal of Power Sources*, vol. 196, no. 22, pp. 9398–9406, 2011.
- [29] M. Dubarry and B. Y. Liaw, "Development of a universal modeling tool for rechargeable lithium batteries," *Journal of Power Sources*, vol. 174, no. 2, pp. 856–860, 2007.
- [30] H. He, R. Xiong, X. Zhang, F. Sun, and J. Fan, "State-of-charge estimation of the lithium-ion battery using an adaptive extended Kalman

- filter based on an improved Thevenin model,” *IEEE Transactions on Vehicular Technology*, vol. 60, no. 4, pp. 1461–1469, 2011.
- [31] Y. Tian, B. Xia, W. Sun, Z. Xu, and W. Zheng, “A modified model based state of charge estimation of power lithium-ion batteries using unscented Kalman filter,” *Journal of Power Sources*, vol. 270, pp. 619–626, 2014.
- [32] P. Mauracher and E. Karden, “Dynamic modelling of lead/acid batteries using impedance spectroscopy for parameter identification,” *Journal of Power Sources*, vol. 67, no. 1-2, pp. 69–84, 1997.
- [33] K. Goebel, B. Saha, A. Saxena, J. R. Celaya, and J. P. Christophersen, “Prognostics in battery health management,” *IEEE Instrumentation & Measurement Magazine*, vol. 11, no. 4, 2008.
- [34] C. Birkl and D. Howey, “Model identification and parameter estimation for LiFePO<sub>4</sub> batteries,” in *Proceedings of IET Hybrid and Electric Vehicles Conference*, 2013, pp. 1–6.
- [35] T. Hu and H. Jung, “Simple algorithms for determining parameters of circuit models for charging/discharging batteries,” *Journal of Power Sources*, vol. 233, pp. 14–22, 2013.
- [36] Z. He, G. Yang, and L. Lu, “A parameter identification method for dynamics of lithium iron phosphate batteries based on step-change current curves and constant current curves,” *Energies*, vol. 9, no. 6, p. 444, 2016.
- [37] J. Yang, B. Xia, Y. Shang, W. Huang, and C. Mi, “Improved battery parameter estimation method considering operating scenarios for HEV/EV applications,” *Energies*, vol. 10, no. 1, p. 5, 2016.
- [38] N. Tian, Y. Wang, J. Chen, and H. Fang, “On parameter identification of an equivalent circuit model for lithium-ion batteries,” in *Control Technology and Applications (CCTA), 2017 IEEE Conference on*. IEEE, 2017, pp. 187–192.
- [39] T. Feng, L. Yang, X. Zhao, H. Zhang, and J. Qiang, “Online identification of lithium-ion battery parameters based on an improved equivalent-circuit model and its implementation on battery state-of-power prediction,” *Journal of Power Sources*, vol. 281, pp. 192–203, 2015.
- [40] G. K. Prasad and C. D. Rahn, “Model based identification of aging parameters in lithium ion batteries,” *Journal of Power Sources*, vol. 232, pp. 79–85, 2013.
- [41] M. Sitterly, L. Y. Wang, G. G. Yin, and C. Wang, “Enhanced identification of battery models for real-time battery management,” *IEEE Transactions on Sustainable Energy*, vol. 2, no. 3, pp. 300–308, 2011.
- [42] L. Zhang, L. Wang, G. Hinds, C. Lyu, J. Zheng, and J. Li, “Multi-objective optimization of lithium-ion battery model using genetic algorithm approach,” *Journal of Power Sources*, vol. 270, pp. 367–378, 2014.
- [43] M. A. Rahman, S. Anwar, and A. Izadian, “Electrochemical model parameter identification of a lithium-ion battery using particle swarm optimization method,” *Journal of Power Sources*, vol. 307, pp. 86–97, 2016.
- [44] Z. Yu, L. Xiao, H. Li, X. Zhu, and R. Huai, “Model parameter identification for lithium batteries using the coevolutionary particle swarm optimization method,” *IEEE Trans. Ind. Electron*, vol. 64, no. 7, pp. 5690–5700, 2017.
- [45] D. W. Limoge and A. M. Annaswamy, “An adaptive observer design for real-time parameter estimation in lithium-ion batteries,” *IEEE Transactions on Control Systems Technology*, 2018, in press.
- [46] Y. Hu and S. Yurkovich, “Linear parameter varying battery model identification using subspace methods,” *Journal of Power Sources*, vol. 196, no. 5, pp. 2913–2923, 2011.
- [47] Y. Li, C. Liao, L. Wang, L. Wang, and D. Xu, “Subspace-based modeling and parameter identification of lithium-ion batteries,” *International Journal of Energy Research*, vol. 38, no. 8, pp. 1024–1038, 2014.
- [48] R. Relan, Y. Firouz, J. Timmermans, and J. Schoukens, “Data-driven nonlinear identification of li-ion battery based on a frequency domain nonparametric analysis,” *IEEE Transactions on Control Systems Technology*, vol. 25, no. 5, pp. 1825–1832, 2017.
- [49] M. J. Rothenberger, D. J. Docimo, M. Ghanaatpishe, and H. K. Fathy, “Genetic optimization and experimental validation of a test cycle that maximizes parameter identifiability for a Li-ion equivalent-circuit battery model,” *Journal of Energy Storage*, vol. 4, pp. 156–166, 2015.
- [50] S. Park, D. Kato, Z. Gima, R. Klein, and S. Moura, “Optimal input design for parameter identification in an electrochemical Li-ion battery model,” in *Proceedings of American Control Conference*, 2018, pp. 2300–2305.
- [51] F. Giri and E.-W. Bai, *Block-Oriented Nonlinear System Identification*. Springer, 2010, vol. 1.
- [52] A. Hagenblad, L. Ljung, and A. Wills, “Maximum likelihood identification of Wiener models,” *Automatica*, vol. 44, no. 11, pp. 2697 – 2705, 2008.
- [53] L. Vanbeylen, R. Pintelon, and J. Schoukens, “Blind maximum-likelihood identification of Wiener systems,” *IEEE Transactions on Signal Processing*, vol. 57, no. 8, pp. 3017–3029, 2009.
- [54] S. Dey, S. Mohon, B. Ayalew, H. Arunachalam, and S. Onori, “A novel model-based estimation scheme for battery-double-layer capacitor hybrid energy storage systems,” *IEEE Transactions on Control Systems Technology*, vol. 27, no. 2, pp. 689–702, 2019.
- [55] A. Mamun, A. Sivasubramaniam, and H. Fathy, “Collective learning of lithium-ion aging model parameters for battery health-conscious demand response in datacenters,” *Energy*, vol. 154, pp. 80–95, 2018.
- [56] D. Andre, M. Meiler, K. Steiner, C. Wimmer, T. Soczka-Guth, and D. Sauer, “Characterization of high-power lithium-ion batteries by electrochemical impedance spectroscopy. I. Experimental investigation,” *Journal of Power Sources*, vol. 196, no. 12, pp. 5334–5341, 2011.
- [57] M. Dubarry, N. Vuillaume, and B. Y. Liaw, “From single cell model to battery pack simulation for Li-ion batteries,” *Journal of Power Sources*, vol. 186, no. 2, pp. 500–507, 2009.
- [58] M. Sitterly, L. Y. Wang, G. G. Yin, and C. Wang, “Enhanced identification of battery models for real-time battery management,” *IEEE Transactions on Sustainable Energy*, vol. 2, no. 3, pp. 300–308, 2011.
- [59] A. Hagenblad, “Aspects of the identification of Wiener models,” Ph.D. dissertation, Linköping University, 1999.
- [60] S. Wright and J. Nocedal, *Numerical Optimization*, 1999, vol. 35, no. 67–68.
- [61] “The EPA Urban Dynamometer Driving Schedule (UDDS) [Online].” Available: <https://www.epa.gov/sites/production/files/2015-10/uddscol.txt>.